Nanoparticle-Mediated Electron Transfer Across Ultrathin Self-Assembled Films

Jianjun Zhao, Christopher R. Bradbury, Sonja Huclova, Inga Potapova, Michel Carrara, and David J. Fermín*

Departement für Chemie und Biochemie, Universität Bern, Freiestrasse 3, CH-3012 Bern, Switzerland

Received: July 26, 2005; In Final Form: October 7, 2005

The electrochemical behavior of arrays of Au nanoparticles assembled on Au electrodes modified by 11-mercaptoundecanoic acid (MUA) and poly-L-lysine (PLYS) was investigated as a function of the particle number density. The self-assembled MUA and PLYS layers formed compact ultrathin films with a low density of defects as examined by scanning tunneling microscopy. The electrostatic adsorption of Au particles of 19 ± 3 nm on the PLYS layer resulted in randomly distributed arrays in which the particle number density is controlled by the adsorption time. In the absence of the nanoparticles, the dynamics of electron transfer involving the hexacynoferrate redox couple is strongly hindered by the self-assembled film. This effect is primarily associated with a decrease in the electron tunneling probability as the redox couple cannot permeate through the MUA monolayer at the electrode surface. Adsorption of the Au nanoparticles dramatically affects the electron-transfer dynamics even at low particle number density. Cyclic voltammetry and impedance spectroscopy were interpreted in terms of classical models developed for partially blocked surfaces. The analysis shows that the electron transfer across a single particle exhibits the same phenomenological rate constant of electron transfer as for a clean Au surface. The apparent unhindered electron exchange between the nanoparticles and the electrode surface is discussed in terms of established models for electron tunneling across metal−insulator−metal junctions.

Introduction

The functionalization of electrode surfaces by two- and three-dimensional (3D) arrays of nanostructures is a fundamental step toward the construction of novel nano-optoelectronic devices.[1−4] The electrostatic assembly of nanomaterials on functionalized surfaces is a versatile approach for generating monodispersed 2D arrays. Surface functionalization can be performed by self-assembly of ionic species of a particular charge onto the substrate. Onto this charged surface, species of the opposite charge can be adsorbed, such as the protecting shell of the nanostructures. Alternative methods involve covalent bonding via bifunctional linkers such as dithiols[5−10] and van der Waals interactions in the case of alkyl stabilized partices.[11−14] Despite significant progress on the synthesis of functionalized nanoparticles and on the formation of organized assemblies on electrodes, only a handful of publications have dealt with key aspects such as how the electrochemical behavior of the ensemble is affected by the nature of the particle−substrate linking units and the particle number density.[15]

Electron transfer from metal nanoparticles to electrode surfaces has been investigated by cyclic voltammetry, impedance spectroscopy, differential pulse voltammetry, potential step chronoamperometry, and rotating disk electrodes.[16−18] Murray and co-workers estimated electron-transfer rate constants in the range of 40 to 160 s^{-1} between gold nanoparticles linked to metal surfaces with a configuration particle−mercaptoundecanoic acid−zinc ion−mercaptoundecanoic acid−surface.[17] Chen and Pei employed dithiols groups adsorbed on Au nanoparticles as linkers to Au surfaces, finding rate constants in a similar range.[18] These authors also observed a strong dependence of the rate constant on the length of alkyl chain of the dithiol, resulting in a coupling coefficient of 0.8 to 0.9 $Å^{-1}$. Horswell et al. studied the dynamics of electron transfer to assemblies of Pt nanoparticles on Au electrodes derivatized with diisocyanooctane monolayers.[16] That report concluded that the *apparent* heterogeneous rate constant in the presence of a monolayer of nanoparticles was approximately four times smaller than that for the clean Au electrode. Several reports have recently been published on the electrochemical behavior of nanoparticles electrostatically adsorbed on metal surfaces,[19−23] however, very little information has been gathered on the dynamics of electron transfer in these systems.

In the present paper, the kinetics of electron transfer involving the ferri/ferrocyanide redox couple is investigated at assemblies of Au nanoparticles electrostatically attached to gold surfaces via an ultrathin self-assembling film comprised of 11-mercaptoundecanoic acid (MUA) and poly-L-lysine (PLYS). As illustrated in Chart 1, the film is formed at the surface by sequential adsorption of a MUA monolayer followed by electrostatic adsorption of PLYS on the ionized carboxyl-terminated surface.[21] The electrochemical responses as a function of the number density of particles adsorbed on MUA−PLYS assemblies are studied by cyclic voltammetry and impedance spectroscopy.

Experimental Section

Chemicals. 11-Mercaptoundecanoic acid 95% (MUA), poly-L-lysine hydrobromide (Mw, 62140) (PLYS), hydrogen tetrachloroaurate(III) hydrate ($HAuCl_4 \cdot 3H_2O$, 99.999%), and sodium citrate dihydrate ($C_6H_5Na_3O_7 \cdot 2H_2O$, 99%) were purchased from Sigma-Aldrich. Potassium ferrocyanide ($K_4Fe(CN)_6 \cdot 3H_2O$), potassium ferricyanide ($K_3Fe(CN)_6$), and Na_2SO_4 anhydrous GR reagents were all purchased from Merck. All the chemicals were

* To whom correspondence should be addressed. Tel: +41 31 6314317. Fax: +41 31 6313994. E-mail: david.fermin@iac.unibe.ch.

10.1021/jp054127s CCC: $30.25
Published on Web 11/11/2005

CHART 1. Schematic Representation of the Nanoparticle Array on the MUA−PLYS-Modified Au Electrode

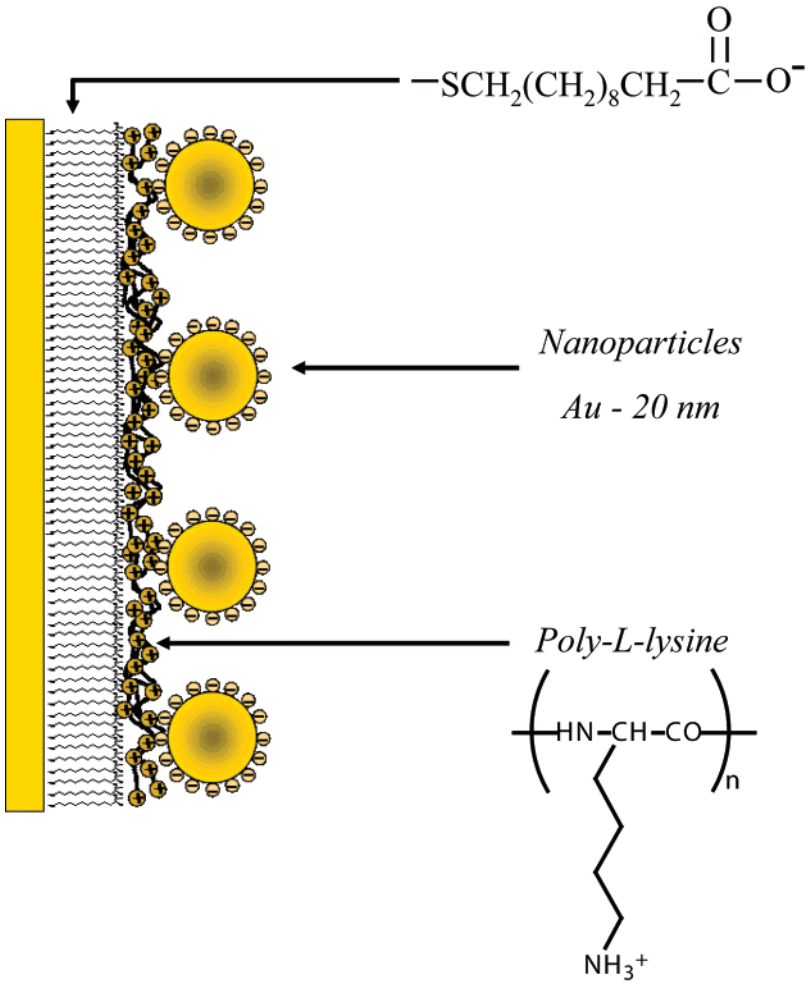

used as received. Millipore filtered ultrapure water (MilliQ water, resistivity >18 MΩ/cm) was used to prepare all aqueous solutions and for rinsing.

Synthesis of Au Nanoparticles. The gold nanoparticles were synthesized in aqueous solution by the reduction of 2.5×10^{-4} mol dm^{-3} $HAuCl_4 \cdot 3H_2O$ (190 cm^3) in the presence of 10 cm^3 of 1% (w/w) trisodium citrate for 1 h under reflux and strong stirring.[1] The core diameter obtained from this method is 19 ± 3 nm as estimated from acoustic AFM images on PLYS-modified mica surfaces.

Gold Electrodes. The gold electrodes were prepared by thermal evaporation of gold onto glass slides at a pressure of less than 2×10^{-8} mbar. First, the glass slides were cleaned by sequential sonication in ethanol and MilliQ water three times for 15 min each, followed by drying under a stream of high-purity N_2. The film growth was initiated by the evaporation of a 1 nm thick chromium layer at 0.1 nm s^{-1} to enhance the adhesion of the gold layer. The gold film was initially grown at a rate of 0.1 nm s^{-1} up to 5 nm, and subsequently, a layer of 200 nm was grown at 1.5 nm s^{-1}. This method provides reproducible disposable polycrystalline gold electrodes featuring grain boundaries of 30 ± 20 nm diameter and a strong (111) orientation as analyzed by AFM and XRD, respectively. The electrochemical behavior after each modification step was investigated using no less than three fresh gold electrodes to add statistical weight to the measurement. The disadvantage of these electrodes is that the topography of the grain boundaries can introduce difficulties in the topographic characterization of the nanoparticle assemblies.

The structure of the MUA−PLYS assembly was examined by STM on atomically flat Au(111) terraces. Gold films were supplied by Arrandee and were annealed with a hydrogen flame prior to surface modification.

Layer-by-Layer Preparation of the Nanostructured Electrodes. The preparation of the MUA−PLYS films was performed following previously reported methods.[24−27] First, the freshly evaporated gold film electrodes were immersed into 10^{-3} mol dm^{-3} MUA solution in ethanol for over 12 h. The excess of MUA was removed by rinsing with a large amount of absolute ethanol and MilliQ water. Subsequently, the modified gold electrode was immersed into 1 mg cm^{-3} of PLYS (pH = 6.0) for 20 min. The modified electrodes were rinsed with copious amounts of MilliQ water and dried under a high-purity N_2 flow.

The adsorption of the citrate-stabilized nanoparticles occurs by electrostatic interaction with the PLYS-terminated films. The number density of particles was controlled by the time of immersion of the modified electrode in colloidal solution.[21,28]

Electrochemical Measurement. Electrochemical measurements were performed in a single compartment cell. The area of the working electrode, 0.071 cm^2, was controlled using chemically inert adhesive Teflon tape (3 M). A platinum foil of 0.34 cm^2 and a saturated calomel electrode (SCE) were used as counter and reference electrodes, respectively. All potentials in this paper are referred to the SCE. The measurements were carried out in a 0.1 mol dm^{-3} Na_2SO_4 solution containing 1×10^{-3} mol dm^{-3} $K_4Fe(CN)_6$ and 1×10^{-3} mol dm^{-3} $K_3Fe(CN)_6$. The solution was purged with nitrogen for 30 min before each

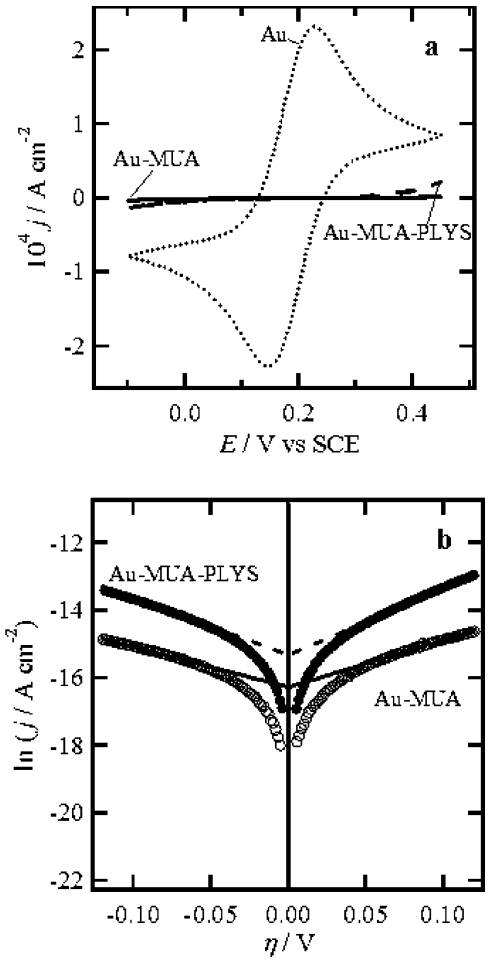

Figure 1. Cyclic voltammograms of the clean Au electrode modified by MUA and PLYS at 50 mV s^{-1} in the presence of 1 mol dm^{-3} $K_4Fe(CN)_6/K_3Fe(CN)_6$: (a) Tafel plots of the same Au−MUA and Au−MUA−PLYS electrodes (b).

measurement. Cyclic voltammograms (CV) and electrochemical impedance spectra (EIS) were measured with an Autolab PGSTAT30 featuring a frequency response analyzer module (Eco Chemie B. V., The Netherlands). The impedance spectra were recorded at the equilibrium potential, $E_{eq} = 0.186 \pm 0.005$ V, between the frequency range of 30 kHz to 130 mHz, with 10 frequency steps per decade and an amplitude of 10 mV rms.

Topographic Characterization of the Assembly. The number density of particles adsorbed on single PLYS films was examined by SEM (ESEM-FEG Philips XL30) at an accelerating voltage of 25 kV. For assemblies of Au particles with a core diameter of 20 nm, SEM allows imaging of large portions of the surface providing accurate determinations of the particle number density. Topographic studies of the MUA−PLYS layer on Au(111) terraces were performed with a scanning tunneling microscope PICO-SPM (Molecular Imaging) in constant current mode. The experiments were conducted at 22 °C and 50% relative humidity.

Results and Discussion

Electrochemical Properties of Au Electrodes Modified by MUA and PLYS. The voltammetric responses in the presence of $K_4Fe(CN)_6/K_3Fe(CN)_6$ for freshly evaporated gold electrodes and after adsorption of MUA and PLYS are displayed in Figure 1a. As reported in previous works,[21,29,30] the MUA self-assembled monolayer brings about a substantial decrease in the electrochemical reactivity. An increase in the current density is observed upon the deposition of the PLYS film on the MUA monolayer. In the potential range of 120 mV around the equilibrium potential, $E_{eq} = 0.186 \pm 0.005$ V, the current−voltage relationship can be described by the classical Butler−Volmer expression

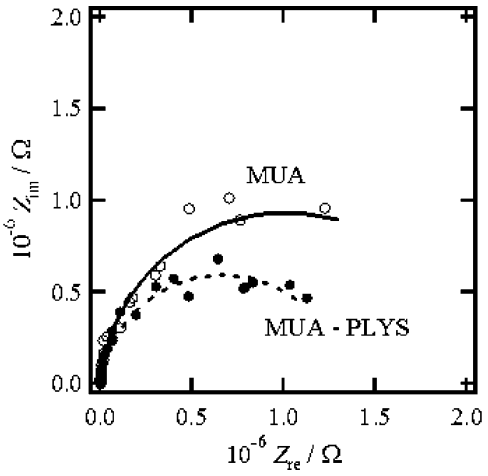

Figure 2. Complex plane impedance plots of the modified Au electrodes at equilibrium potential (0.186 V). The frequency was swept from 13 kHz to 0.13 Hz, and the modulation amplitude was 10 mV rms. The continuous lines correspond to fits to the Randles equivalent circuit.

$$i = i_o[e^{\alpha\frac{nF}{RT}\eta} - e^{-(1-\alpha)\frac{nF}{RT}\eta}] \quad (1)$$

where the exchange current i_o and the overpotential η are given by

$$i_o = nFAk_o(c_{red})^{1-\alpha}(c_{ox})^{\alpha} \quad (2)$$

$$\eta = (E - E_{eq}) \quad (3)$$

The parameters A, k_o, and α correspond to the electrode area, the electron-transfer rate constant at the equilibrium potential, and the transfer coefficient, respectively.

The exchange current density ($j_o = i_o/A$) was estimated from Tafel plots as illustrated in Figure 1b. The MUA-modified electrode provided a value of $j_o = (8.7 \pm 0.5) \times 10^{-8}$ A cm^{-2}, while in the presence of the PLYS film j_o was $(2.2 \pm 0.5) \times 10^{-7}$ A cm^{-2}. Most of the current potential curves can be described by a transfer coefficient of 0.5 ± 0.1, although the potential dependence for the MUA-modified electrode was not ideal. The apparent "increment" of the electron-transfer rate constant induced by the PLYS film can be rationalized in terms of (i) an increase in the interfacial concentration of the anionic redox species due to a strong affinity to the polycationic film or (ii) by an increase in defects of the self-assembled film exposing active sites at the electrode surface.

The results obtained from the Tafel plots were further confirmed by impedance spectroscopy at the equilibrium potential. Typical impedance spectra obtained for the MUA and MUA−PLYS-modified electrodes are illustrated in Figure 2 as Nyquist plots. The continuous lines correspond to fits to the Randles equivalent circuit, from which average charge-transfer resistances of $(3.2 \pm 1.0) \times 10^6$ and $(1.8 \pm 1.0) \times 10^6$ Ω were obtained for the MUA and MUA−PLYS modifications, respectively. The exchange current, as defined by eq 2, is related to

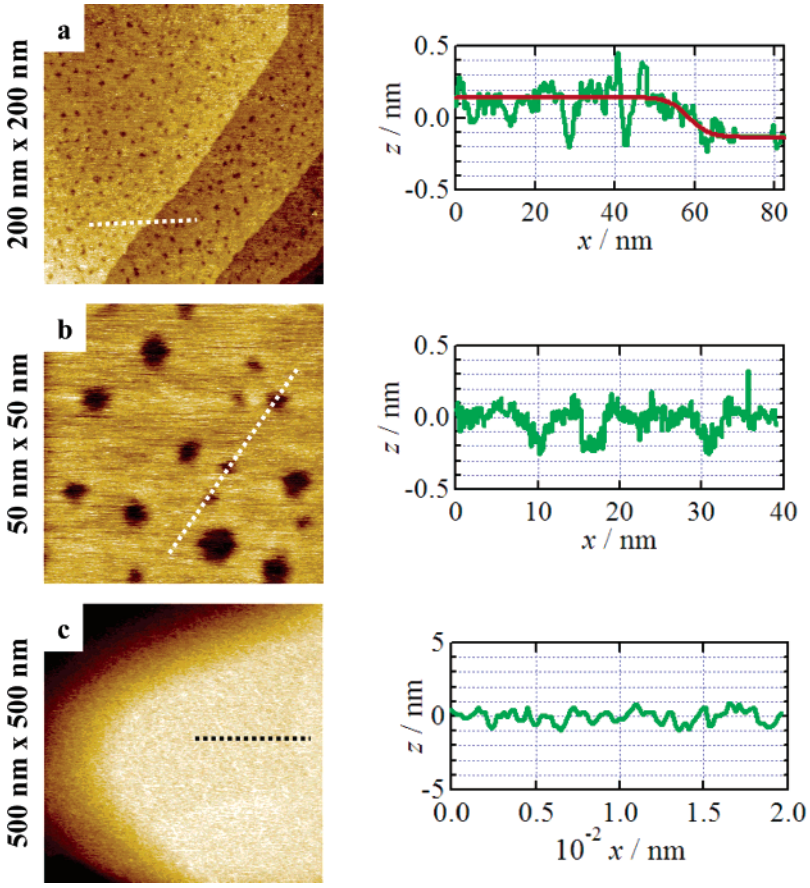

Figure 3. STM images of the MUA self-assembly monolayer on Au(111) terraces at (a) −0.9 V and 2 pA and (b) −0.9 V and 10 pA. The cross sections in both figures confirm that the pits depth is equal to the monatomic step height at the Au(111) surfaces. (c) STM image of MUA−PLYS on the same Au(111) sample at 1.5 V and 1.5 pA.

the charge-transfer resistance (R_{ct}) at the equilibrium potential by

$$R_{ct} = RT/nFi_o \quad (4)$$

Upon normalization to the electrode surface area, the exchange current densities as estimated from the impedance spectra and eq 4 for MUA and MUA−PLYS-modified electrodes were (1.1 ± 0.4) × 10^{-7} and (2.0 ± 1.0) × 10^{-7} A cm^{-2}, respectively. These values are consistent with those obtained from the Tafel plots illustrated in Figure 1b.

To further investigate the effect of the surface modification on the dynamics of electron transfer, the structure of assembly was investigated by ex-situ STM at constant current on Au(111) surfaces. The MUA monolayer structure in parts a and b of Figure 3 shows extended compact domains as well as the characteristic thiol "pits". The profiles traced on parts a and b of Figure 3 confirm that the pits' depth corresponds to one (in some cases two) atomic step of Au(111). Ordered MUA molecules are also present at the bottom of the pits; consequently, these pits cannot be regarded as defects exposing a bare Au surface to the electrolyte solution.[30,31] Although molecular resolution of the MUA monolayer has been reported by several authors,[32−34] no clear ordering is observed in these images most probably due to hydrogen bonding through the carboxylate end group. We also use tip currents below 10 pA and bias around −1 V in order to minimize changes in the structure of the layer induced by the STM tip.

The topography of the PLYS film on the MUA-modified Au surface appears rather featureless as exemplified in Figure 3c. Over large flat domains, no topographic features associated with the thiol pits, atomic steps, or any structure larger than 1 nm can be observed. Although STM images confirm the homogeneous and extensive coverage of the surface by PLYS, very little information can be extracted concerning the layer thickness. Qualitative analysis of the surface topography indicates that the layer thickness is greater than 0.25 nm because the Au(111) monatomic steps are no longer visible. Corn and co-workers concluded from SPR studies that the MUA−PLYS layer thickness is of the order of 1 nm.[24]

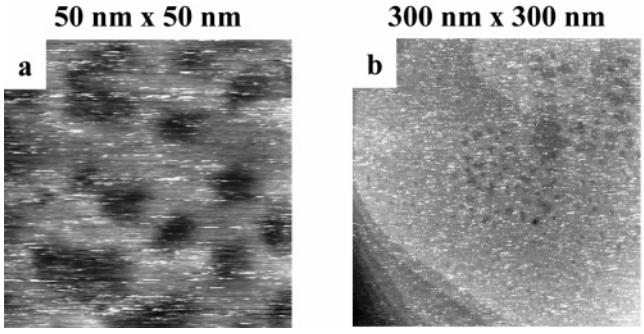

Figure 4. (a) STM image of the MUA−PLYS on Au(111) obtained at −0.5 V and 500 pA. Under these tunneling conditions, the tip is inside the film, exposing the underlying MUA layer. (b) The same section of the surface but with a wider scanned area and tunneling parameters −1.0 V and 1 pA. Increasing the tip−substrate distance with respect to (a) allows us to image the removal of the PLYS films at high tunneling conditions.

The image displayed in Figure 4a was obtained with 500 pA and −0.5 V tunneling current and bias, respectively. Under these conditions, the tip penetrates into the PLYS film and reveals

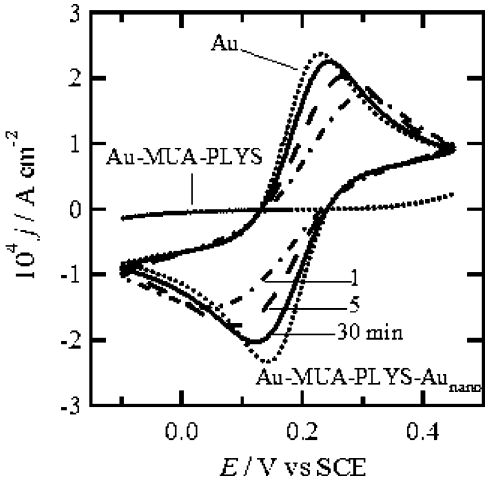

Figure 5. Cyclic voltammograms as a function of the adsorption time of the Au nanoparticles. The responses corresponding to the clean and modified Au surface are also displayed for comparison. Significant changes are observed even after 1 min adsorption time.

the thiol pits of the underlying MUA monolayer. The pit density and size appear larger than in parts a and b of Figure 3, which may originate from defects induced by the STM tip operating at high currents and lower voltages. Further scans at 10 pA and −1V reveal the modification of the PLYS layer induced by the tip at high currents as exemplified in Figure 4b. The contrast in the topography between the areas perturbed and nonperturbed by the STM confirms that the PLYS film covers the MUA monolayer.

The sequence of STM images in Figures 3 and 4 can be taken as evidence that the increase of the apparent electron-transfer rate constant in the presence of PLYS is connected to an enhancement of the interfacial concentration of the anionic redox couple, rather than due to the formation of *active sites* on the Au electrode. Willner and co-workers reached the same conclusion from the alternating behavior of the apparent electron-transfer constant upon electrostatic adsorption of polyanions and polycations.[35] In addition, our previous studies employing the hydrophobic probe ferrocene in 1,2-dichloroethane provided high charge-transfer resistance for the PLYS-terminated surface.[21] Similar effects have also been observed on self-assembled monolayers featuring terminating groups of different charges.[29]

Dynamic of Electron Transfer as a Function of the Number Density of Nanoparticles. Voltammetric responses in the presence of ferri/ferrocyanide after various times of adsorption of Au nanoparticles are exemplified in Figure 5. As mentioned in the previous section, each measurement was performed on a freshly modified Au electrode. It is observed that the current−potential relationship is dramatically affected even after 1 min of deposition. The peak-to-peak separation decreases while the current density increases as the time of deposition is increased up to 30 min. A deposition time of up to 4 h shows no significant changes in the cyclic voltammograms. These results clearly indicate that the decoration of PLYS-terminated layers with gold nanoparticles brings about a significant increase in the rate of electron transfer. This observation has been reported for similar systems, although only qualitative analyses have been presented.[21,22] To study these phenomena in a more quantitative fashion, the number density of particles as a function of the deposition time must be considered.

The increase in the number density of Au nanoparticles with increasing adsorption time can be visualized in the SEM images shown in Figure 6. Well-monodispersed arrays with very low density of defects are observed for adsorption times as long as 4 h. Particle counting and distribution analysis were performed using Matlab.[36] Caution was taken to eliminate the topographic features of the underlying substrate in the particle counting.

The particle number density (Γ_{Au}) as a function of the adsorption time is illustrated in Figure 7. In agreement with our previous report,[21] the adsorption kinetics can be described in terms of a fixed number of adsorption sites (N) and coverage independent adsorption (k_a) and desorption (k_d) rate constants. Under this assumption, the time dependence of Γ_{Au} is given by

$$\Gamma_{Au} = N\frac{k_a}{k_a + k_d}[1 - \exp(-(k_a + k_d)t)] \qquad (5)$$

where the phenomenological rate constant k_a is linearly dependent on the concentration of the particles in solution. The dashed line in Figure 7 was obtained from eq 5 by taking the first term as $(4.2 \pm 0.1) \times 10^{10}$ cm^{-2} and the exponential term as $(3.3 \pm 0.6) \times 10^{-4}$ s^{-1}. If we assume that $k_a \gg k_d$, then the former parameter corresponds to the number density of active sites, while the latter is the pseudo-first-order rate constant for particle adsorption.

From the dynamics of particle adsorption, it becomes clear that the electrochemical responses of the modified electrode are strongly affected by the particle number density at the electrode surface. For instance, substantial changes in the cyclic voltammogram are observed upon adsorption of nanoparticles for 1 min, which corresponds to $\Gamma_{Au} = 8.23 \times 10^8$ cm^{-2} and a fractional coverage of the electrode surface of 0.23% (taking into account an average radius of 9.5 nm). The voltammetric behavior can be rationalized within the framework of the model developed by Amatore et al. for partially covered electrodes.[37] This model described the nonlinear diffusion profiles in the case that the size of the electroactive sites and the distance separating them is smaller than the thickness of the diffusion layer. Considering that the average center-to-center distance lies between 40 and 100 nm for different particle coverages,[36] the model predicts that the peak currents are of the same magnitude as for the "unblocked" electrode and the peak-to-peak separation increases with the decrease in density of the electroactive sites. This behavior is observed for deposition times higher than 5 min, where the fraction of the surface covered by nanoparticles is above 1.1%. At a shorter time of deposition, the peak currents decrease and the voltammetric responses adopt a quasi-sigmoidal shape. This behavior suggests the convolution between planar and spherical diffusion profiles as the particle number density is rather low.

In the limit where the peak currents show a weak dependence on the particle coverage, it is expected that the apparent electron-transfer rate constant (k_{Au}^{ap}) is linearly dependent on the fractional surface coverage of the Au nanoparticles (θ_{Au})[37,38]

$$k_{Au}^{ap} = k_{Au}^{ap,max}\theta_{Au} = k_{Au}^{ap,max}\Gamma_{Au}\pi(r_{Au})^2 \qquad (6)$$

where $k_{Au}^{ap,max}$ corresponds to the limiting value for unity fractional coverage and r_{Au} is the average radius of the nanoparticles. In eq 6, the dimensionality of the Au particles is reduced from spheres to a disk projection on the modified-electrode surface. The rationale behind this assumption is based on the characteristic transition time from spherical-to-planar diffusion. Previous estimations based on the Scharifker model[39] indicate that this transition takes place in the sub-microsecond time domain considering the size and number density of the

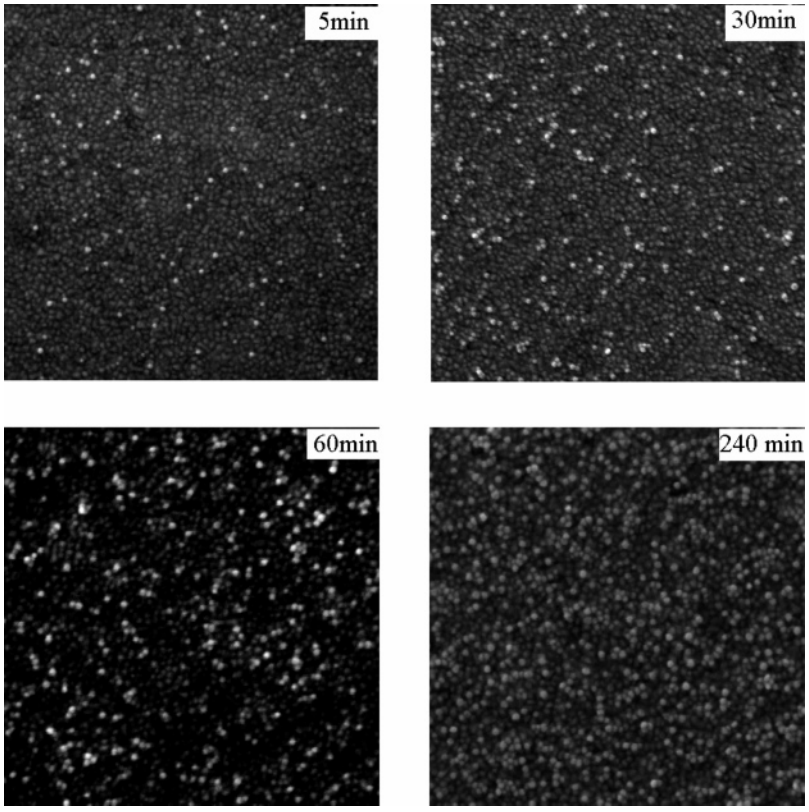

Figure 6. 2.0 μm $\times$ 2.0 μm SEM images obtained at different deposition time. The background topography corresponds to the grain boundaries of the Au electrode. The particle number density as a function of deposition time was obtained by digital analysis of several samples.

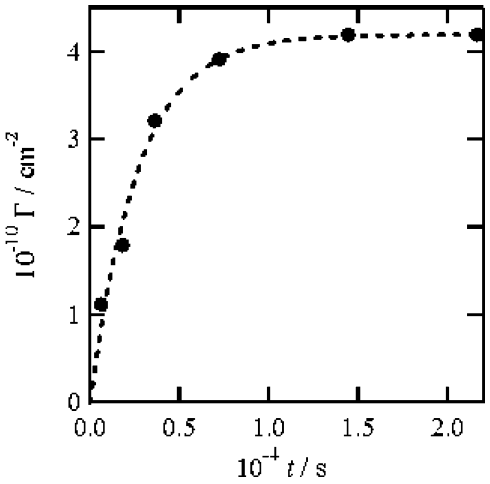

Figure 7. Particle number density as a function of the adsorption time. The continuous lines correspond to the fit to a model based on kinetically controlled adsorption on a fixed number of active sites.

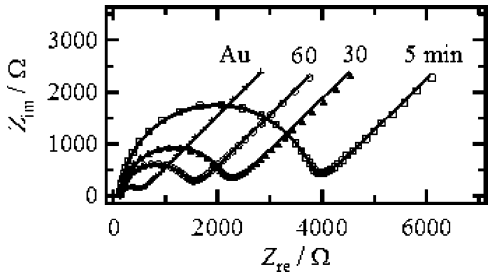

Figure 8. Complex impedance spectra of the modified electrode as a function of the nanoparticle adsorption time. These spectra can be contrasted to the behavior of the clean Au surface (labeled as Au) and after modification by MUA and PLYS (Figure 2). Continuous lines are associated with the modified Randles circuit illustrated in Chart 2.

nanoparticles.[21] This assumption is also consistent with the previous analysis of the cyclic voltammograms based on the Amatore model.[37]

To evaluate the apparent rate constant as a function of the particle number density, impedance spectra were recorded at the formal transfer potential. The complex representation of the impedance spectra in Figure 8 shows that the magnitude of the high frequency semicircle decreases as the adsorption time increases. Even at short adsorption times, the impedance responses are significantly smaller than the values obtained in the absence of Au nanoparticles (cf. Figure 2). On the other hand, the magnitude of the impedance of the nanostructured electrodes was higher than that for the clean Au surface even at the maximum particle density number. Qualitatively, this trend is consistent with the behavior expected from eqs 2, 4, and 6, that is, as the particle number density increases the apparent electron-transfer rate constant increases and the charge-transfer resistance decreases.

The analysis of the impedance spectra was performed with a modified Randles circuit illustrated in Chart 2, in which electron transfer mediated by the nanoparticles is in parallel to direct electron transfer across the MUA−PLYS layer. As shown below, the charge-transfer resistance across the MUA−PLYS layer (R_{film}) is orders of magnitude higher than that for the nanoparticle-mediated pathway (R_{Au}) and the equivalent circuit can be effectively reduced to the classical Randles scheme. As discussed further below, the resistance R_{Au} contains elements associated with the kinetics of electron exchange between the particle and the redox couple as well as between the particle and the electrode substrate. The equivalent capacitance C_{int} corresponds to a parallel combination of the capacitance associated with film/electrolyte and nanoparticle/electrolyte junctions.[16] Reincke et al. employed a more complex equivalent

CHART 2. Modified Randles Equivalent Circuit for Rationalizing the Impedance Spectra of the Nanostructured Electrode[a]

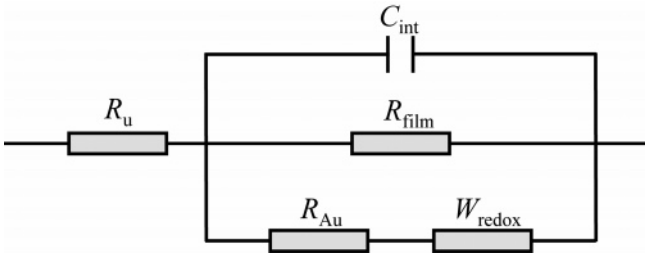

[a] The capacitance C_{int} corresponds to the equivalent capacitor of the whole ensemble which involves contributions from the film/electrolyte and nanoparticle/electrolyte junctions. The parameters R_{film} and R_{Au} correspond to the phenomenological charge-transfer resistances across the MUA−PLYS film and MUA−PLYS−Au(particle), respectively. R_u is the uncompensated resistance, and W_{redox} is the classical Warburg impedance.

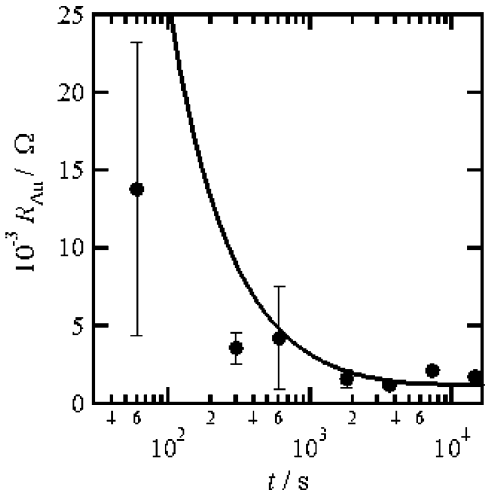

Figure 9. Apparent charge-transfer resistance as a function of the nanoparticle adsorption time. The line corresponds to the theoretical behavior for an array of Au nanoelectrodes with a time-dependent number density (see text).

circuit in which the electron discharge across the film in contact with the nanoparticle occurs at a different time scale than at the particle/solution boundary.[40] The continuous line in Figure 8 confirms that the impedance spectra can be fitted with this equivalent circuit employing the Warburg elements derived from measurements on clean Au surfaces. As expected from the voltammetric analysis, the low-frequency limit of the impedance spectra is controlled by planar diffusion of the redox species to the nanostructured electrode.

The effective charge-transfer resistance R_{Au} estimated from the impedance spectra is displayed in Figure 9 as a function of the nanoparticle adsorption time. As mentioned previously, R_{Au} decreases with increasing adsorption times. It is also observed that the standard deviation for several measurements substantially increases toward short adsorption times. The reason behind this effect is related to the strong dependence of this parameter on the particle number density. As illustrated in Figure 7, Γ_{Au} is highly dependent on the adsorption time and uncertainties in the range of a few seconds, as well as variations in the density of active adsorption sites for different electrodes, can have a dramatic effect on the electrochemical responses. As the particle number density becomes less dependent on the adsorption time, above 10 min, the relative error values are less than 10%.

From eqs 2 and 4−6, the resistance R_{Au} can be expressed in terms of

$$R_{Au} = \frac{RT}{nFi_{Au}} = \frac{RT}{n^2F^2k_{Au}^{ap}Ac} = \frac{RT}{n^2F^2k_{Au}^{ap,max}\Gamma_{Au}\pi(r_{Au})^2Ac} \quad (7)$$

taking the transfer coefficient as 0.5. The dependence of R_{Au} on the nanoparticle adsorption time is given by the adsorption kinetics described by eq 5. The continuous line in Figure 9 corresponds to a fit of the experimental data employing the adsorption kinetics estimated from Figure 7. The parameter $k_{Au}^{ap,max} = 0.017 \pm 0.005$ cm s^{-1} is obtained following this fit. This value is rather close to the value obtained for *polycrystalline Au electrodes* as exemplified in Figure 8, that is, 0.012 ± 0.001, and within the range of 0.010−0.035 cm s^{-1} reported by several authors.[41−44] It should also be mentioned that impedance measurements on clean Au electrodes previously exposed to citrate solutions also showed a similar electron-transfer rate constant.

"Unhindered" Electron Transfer from the Metal Nanoparticles to the Electrode Surface. The results described in the previous section confirmed that the kinetics of electron transfer is significantly decreased upon modification of the Au electrode by the MUA−PLYS layer. However, it was observed that not only the charge-transfer resistance effectively decreases upon an increasing number density of Au nanoparticles but also the electron-transfer rate constant to a single particle is identical to the one observed on bulk polycrystalline Au. These results appear to contrast with previous studies reported by the groups of Murray[17] and Chen,[18] where the dynamics of charge injection to Au nanoparticles were reported. However, it should be noted that these studies involve considerably smaller particles (core diameter below 5 nm) protected by alkane-thiol groups which can introduce a substantial charge-transfer resistance to the particles. In this section, we shall address the issues behind the apparent unhindered electron transfer between the Au particles and the modified-electrode surface. A trivial explanation for this effect is that the Au nanoparticles induce a strong deformation of the ultrathin layer, establishing direct contact with the electrode surface. This situation is graphically illustrated in Chart 3a. However, as discussed below, it is not necessary to invoke a direct electrical contact between the particle and the electrode to account for these experimental results.

Let us first consider the charge-transfer resistance in the absence of nanoparticles. The distance dependence of the electron-transfer rate constant in the presence of the MUA monolayer can be phenomenologically described by

$$k_{MUA} = k_o \exp(-\beta\delta) \quad (8)$$

where δ is the monolayer thickness and k_o is the apparent rate constant of the clean Au electrode. The coupling coefficient β has been estimated for saturated alkane monolayers to be in the range of 0.8−1.2 Å^{-1}.[45−48] Assuming that the increase in charge-transfer resistance in the presence of MUA is mostly related to an increase in the tunneling distance, then eq 8 can be expressed in terms of eqs 2 and 4 as

$$\delta = \beta^{-1} \ln(R_{ct}^{MUA}/R_{ct}) \quad (9)$$

Taking R_{ct} and R_{ct}^{MUA} as 253 and 3.2×10^6 Ω, respectively, (impedance data in Figures 2 and 8), the MUA monolayer thickness can be estimated between 7.8 and 11.8 Å. If the MUA molecules assembled at the surface adopt a fully extended upright position, then the thickness of the monolayer should

CHART 3. Schematic Illustrations of the Surface−Film−Nanoparticle Junction[a]

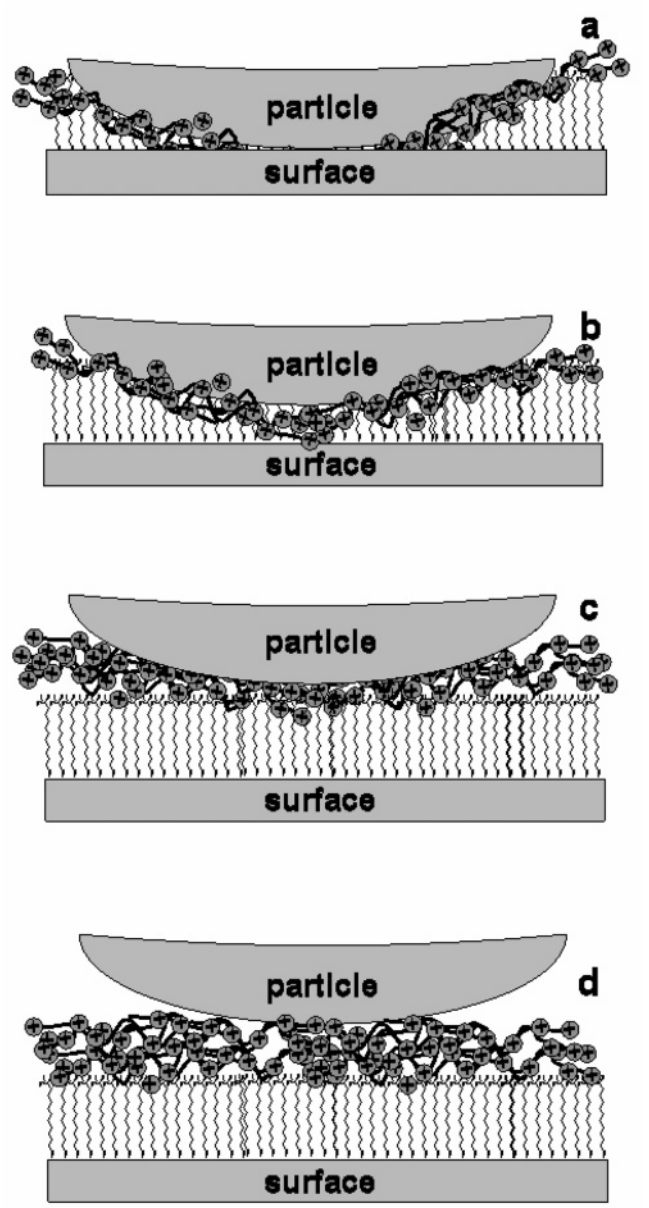

[a] The apparent unhindered electron transfer from the particle to the surface can be interpreted in terms of a physical contact between the particle and the electrode (a). However, the results can also be compatible with the presence of a finite tunneling resistance associated with configurations (b) and (c). A dominant film resistance can be estimated from the configuration (d) which appears inconsistent with the experimental results (see text).

approach values between 16 and 18 Å.[49] Consequently, the barrier thickness estimated from the apparent electron-transfer rate constants can be interpreted as the effective monolayer thickness resulting from a distribution of the orientation of the MUA molecules at the surface.

It should not be totally discarded that defects on the MUA monolayer can also play a role in the estimated values of R_{ct}^{MUA}. We have performed identical measurements on dodecanethiol-modified electrodes, and the charge-transfer resistance is approximately 20 times larger than R_{ct}^{MUA} (results not shown). In addition to the blocking effect induced by the dodecanethiol monolayer, it has been also proposed that a highly hydrophobic region is created at the SAM−electrolyte boundary[50] that may also contribute to the observed charge-transfer resistance. Despite the structural differences induced by the SAM ending group, the comparable charge-transfer resistances observed for MUA and dodecanethiol support the analysis of the electrochemical data in terms of a hindered electron tunneling.

CHART 4. Equivalent Circuit Associated with the Phenomenological Charge-Transfer Resistance R_{Au}[a]

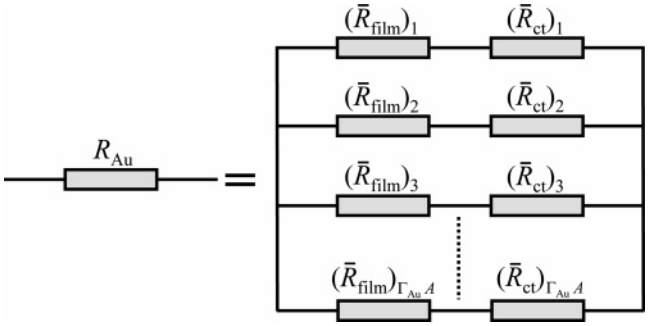

[a] The element $\bar{R}_{ct}$ corresponds to the charge-transfer resistance from the redox species to a single particle, while $\bar{R}_{film}$ is the tunneling resistance from the particle to the electrode surface.

The results in Figures 1 and 2 show that the adsorption of the PLYS layer manifests itself by a decrease in the apparent charge-transfer resistance by a factor of 2. As discussed previously, this behavior indicates that the redox couple effectively permeates through the film leading to an increase in the interfacial concentration with respect to the MUA-modified electrode. Consequently, the electron transfer across the MUA−PLYS assembly remains, to a large extent, controlled by the tunneling across the MUA monolayer. These results are different than those reported by Barriera et al.[51] and Willner et al.,[35] in which the transport of the redox couple through polyelectrolyte films assembled on cysteamine and cystamine-modified Au electrodes provides a significant contribution to the electrochemical impedance. The difference in the electron transfer "blocking" between these short thiols and MUA arises from three aspects: (i) the thickness of the thiol monolayer is significantly larger for MUA, (ii) cysteamine generates more disordered monolayers,[52,53] and (iii) electrostatic interactions between the thiol ending group and the hexacyanoferrate redox couple.

In the presence of the Au nanoparticles (Figures 5 and 8), the electron transfer is channelled through the particles to the electrode surface effectively unhindered by the MUA−PLYS film. On a rather simplified picture, the charge-transfer resistance *per particle* can be expressed as a series of charge-transfer resistances associated with the reorganization energy of the redox couple, that is, $\bar{R}_{ct}$, and the resistance across the film directly underneath the particle $\bar{R}_{film}$. As illustrated in Chart 4, the measured R_{Au} corresponds to the combination of $\bar{R}_{ct}$ and $\bar{R}_{film}$ associated with each individual particle across the electrode surface. This approach considers the macroscopic diffusional impedance as a single element in series with the ensemble of nanoparticles based on the fact that only planar diffusion is observed at all frequencies.

The element $\bar{R}_{film}$ can be initially treated in terms of a single homogeneous barrier of thickness (s) and a coupling factor β. If the barrier characteristics are as observed in the presence of MUA, then s and β can be roughly taken as 10 Å and 1 Å^{-1}, respectively. However, in the case that the barrier includes a significant contribution from the PLYS film itself, then the electron tunneling will occur over a region of up to 20 Å (taken

the PLYS layer as 1 nm thick[24]). Parts b−d of Chart 3 provide a graphical illustration of how the particles can be interacting with the modified surface. In essence, the electronic communication between particles and the electrode surface is determined by the thickness of the barrier associated with the MUA−PLYS film. We shall consider the limiting cases defined by parts c and d of Chart 3, that is, $s \sim 10$ Å (no contribution from the PLYS film to $\bar{R}_{film}$) and $s \sim 20$ Å (estimated thickness for the MUA−PLYS film). For the sake of simplicity, we will assume a constant coupling factor β of 1 Å^{-1}.

On the basis of theories for electron tunneling across metal−insulator−metal junctions,[47,48,54] the current voltage characteristic for a junction of cross section $\bar{A}$ can be expressed as

$$I = \frac{q\bar{A}}{4\pi^2\hbar s^2}\left\{\left(\phi - \frac{qV}{2}\right)\exp\left(-\frac{2s\sqrt{2m}}{\hbar}\sqrt{\phi - \frac{qV}{2}}\right) - \left(\phi + \frac{qV}{2}\right)\exp\left(-\frac{2s\sqrt{2m}}{\hbar}\sqrt{\phi + \frac{qV}{2}}\right)\right\} \quad (10)$$

where ϕ is the energy barrier height, s is the barrier width, and m is the electron mass. Taking the coupling factor β as

$$\beta = 2\sqrt{\frac{2m\phi}{\hbar^2}} \approx 1 \text{ Å}^{-1} \quad (11)$$

the resistance of the junction with an area equivalent to the cross section of *a single nanoparticle* ($\bar{A} = \pi r_{Au}^2$) in the low bias region is given by[48]

$$\bar{R}_{film} = \frac{8\pi^2\hbar s}{q^2\beta}\exp(\beta s) \quad (12)$$

For the two limiting thicknesses mentioned previously, that is, 10 Å $< s <$ 20 Å, eq 12 provides values between 7.1×10^{10} and 3.1×10^{15} Ω, respectively. On the other hand, the element $\bar{R}_{ct}$ can be simply obtained by scaling the macroscopic charge-transfer resistance of a clean Au electrode to the cross section of single particle

$$\bar{R}_{ct} = \frac{RT}{n^2F^2k_{Au}^{ap,max}\pi(r_{Au})^2c} \quad (13)$$

Taking $r_{Au} = 9.5$ nm, it follows from eq 13 that $\bar{R}_{ct} = 5.5 \times 10^{12}$ Ω.

Finally, it follows from the equivalent circuit in Chart 4 that

$$R_{Au} = \left(\left(\frac{1}{\bar{R}_{Au} + \bar{R}_{film}}\right)_1 + \left(\frac{1}{\bar{R}_{Au} + \bar{R}_{film}}\right)_2 + \cdots \left(\frac{1}{\bar{R}_{Au} + \bar{R}_{film}}\right)_{\Gamma_{Au}A}\right)^{-1} = \frac{\bar{R}_{Au} + \bar{R}_{film}}{\Gamma_{Au}A} \quad (14)$$

In the limiting case that $\bar{R}_{Au} \gg \bar{R}_{film}$, eq 7 can be recovered from eqs 13 and 14. This analysis indicates that, although PLYS plays a key role on the organization of the nanoparticles on the electrode surface, this layer has very little contribution to the effective electron-transfer barrier. This conclusion suggests that the structure of the particle−film−metal junction can be represented in terms of parts a−c of Chart 3, that is, the film thickness in contact with the nanoparticles is considerably thinner than 1 nm. However, it could also be possible that the coupling factor associated with tunneling across the polyelectrolyte film is less than 1 Å^{-1}. To uncouple both effects, accurate estimation of the average thickness of the MUA−PLYS film in contact with the particles is required. We are currently investigating in more detail the structure of these films with the aim to be able to control the dynamics of charge injection from particles to the metal electrode.

Conclusions

The sequential self-assembly of MUA and PLYS on Au surfaces generates ultrathin compact films with a homogeneous coverage and very low density of surface defects. This film introduces a strong barrier for electron transfer involving hydrophilic redox species such as hexacyanoferrate. The electron-transfer rate constant at the modified electrode is mainly determined by the effective electron tunneling distance and, to a lesser extent, by electrostatic interactions between the fixed charges at the electrode surface and the redox species in solution.

The electrostatic adsorption of Au nanoparticles from aqueous solution onto the PLYS film exhibits a "Langmuir" type kinetics which allows controlling of the number density of particles at the surface by the adsorption time. Very low densities of aggregates are observed for adsorption times below 2 h. Cyclic voltammograms and impedance spectra are significantly affected by the adsorption of the nanoparticles even at fractional coverage below 1%. The behavior of the electrochemical responses as a function of the number density of particles was interpreted in terms of a well-established model for insulated electrodes featuring nanoscopic active sites. The results confirm that the assembly of Au particles behaves as an array of randomly distributed nanoelectrodes.

The apparent unhindered electron exchange between the nanoparticles and the electrode surface was discussed in terms of electron tunneling across metal−insulator−metal junctions. The analysis shows that the PLYS film has a negligible contribution to the tunneling barrier between the nanoparticles and the electrode surface and the overall kinetics is controlled by the electron exchange between the redox species and the particles. These conclusions have some important consequences for future studies in this kind of nanostructured electrode. For instance, electron-transfer rate constants which are inaccessible on clean metal electrodes can be scaled down to measurable values by carefully controlling the number of particles on modified surfaces. These studies also have opened the way for studying new types of electrocatalysts, as well as templates for electrochemical nucleation of nanocomposites.

Acknowledgment. We acknowledge a number of people who provided valuable support and discussions in the preparation of this work. We are grateful to Prof. Hans Siegenthaler and Dr. Edit Szöcs from the DCB Universität Bern for providing facilities and expertise on the STM measurements. Ms. Beatrice Frey (Universität Bern), Karl Krämer (Universität Bern), and M. Dadras (Université de Neuchâtel) are gratefully acknowledged for the SEM and XRD measurements. We are also indebted to Prof. Willy Lüthy and Mr. Beat Locher from the Department of Physics for their valuable support on the preparation of Au electrodes. Helpful discussions with Prof. Wolfgang Schmickler (Universität Ulm), Prof. Patrick Unwin (University of Warwick), and Prof. M. Cynthia Goh (University of Toronto) are appreciated. Finally, we are grateful to the Swiss National Science Foundation (Projects PP002-68708 and 200021-105238), the Portland-Zementstiftung, and the Stiftung zur Förderung der Wissenschaftlichen Forschung an der Universität Bern for the financial support.

References and Notes

(1) Shipway, A. N.; Katz, E.; Willner, I. *ChemPhysChem* **2000**, *1*, 18.
(2) Willner, I.; Willner, B. *Pure Appl. Chem.* **2002**, *74*, 1773.

(3) Arsenault, A. C.; Halfyard, J.; Wang, Z.; Kitaev, V.; Ozin, G. A.; Manners, I.; Mihi, A.; Miguez, H. *Langmuir* **2005**, *21*, 499.
(4) Angelatos, A. S.; Radt, B.; Caruso, F. *J. Phys. Chem. B* **2005**, *109*, 3071.
(5) Yang, M.; Zhang, Z. *Electrochim. Acta* **2004**, *49*, 5089.
(6) Baum, T.; Bethell, D.; Brust, M.; Schiffrin, D. J. *Langmuir* **1999**, *15*, 866.
(7) Bethell, D.; Brust, M.; Schiffrin, D. J.; Kiely, C. *J. Electroanal. Chem.* **1996**, *409*, 137.
(8) Chen, S. *J. Phys. Chem. B* **2000**, *104*, 663.
(9) Bakkers, E.; Roest, A. L.; Marsman, A. W.; Jenneskens, L. W.; de Jong-van Steensel, L. I.; Kelly, J. J.; Vanmaekelbergh, D. *J. Phys. Chem. B* **2000**, *104*, 7266.
(10) Kulkarni, G. U.; Thomas, R. J.; Rao, C. N. R. *Pure Appl. Chem.* **2002**, *74*, 1581.
(11) Zhang, J.; Lahtinen, R. M.; Kontturi, K.; Unwin, P. R.; Schiffrin, D. J. *Chem. Commun.* **2001**, 1818.
(12) Riley, D. J.; Tull, E. J. *J. Electroanal. Chem.* **2001**, *504*, 45.
(13) Liljeroth, P.; Vanmaekelbergh, D.; Ruiz, V.; Kontturi, K.; Jiang, H.; Kauppinen, E.; Quinn, B. M. *J. Am. Chem. Soc.* **2004**, *126*, 7126.
(14) Roest, A. L.; Houtepen, A. J.; Kelly, J. J.; Vanmaekelbergh, D. *Faraday Trans.* **2003**, *123*, 55.
(15) Leopold, M. C.; Donkers, R. L.; Georganopoulou, D.; Fisher, M.; Zamborini, F. P.; Murray, R. W. *Faraday Trans.* **2003**, *125*, 63.
(16) Horswell, S. L.; O'Neil, I. A.; Schiffrin, D. J. *J. Phys. Chem. B* **2003**, *107*, 4844.
(17) Hicks, J. F.; Zamborini, F. P.; Murray, R. W. *J. Phys. Chem. B* **2002**, *106*, 7751.
(18) Chen, S. W.; Pei, R. J. *J. Am. Chem. Soc.* **2001**, *123*, 10607.
(19) Song, W.; Okamura, M.; Kondo, T.; Uosaki, K. *J. Electroanal. Chem.* **2003**, *554*−*555*, 385.
(20) Yu, A.; Liang, Z.; Cho, J.; Caruso, F. *Nano Lett.* **2003**, *3*, 1203.
(21) Kakkassery, J. J.; Abid, J.-P.; Carrara, M.; Fermín, D. J. *Faraday Trans.* **2004**, *125*, 157.
(22) Sagara, T.; Kato, N.; Nakashima, N. *J. Phys. Chem. B* **2002**, *106*, 1205.
(23) Hicks, J. F.; Seok-Shon, Y.; Murray, R. W. *Langmuir* **2002**, *18*, 2288.
(24) Cheng, Y.; Corn, R. M. *J. Phys. Chem. B* **1999**, *103*, 8726.
(25) Cheng, Y.; Murtomaki, L.; Corn, R. M. *J. Electroanal. Chem.* **2000**, *483*, 88.
(26) Kakkassery, J. J.; Fermín, D. J.; Girault, H. H. *Chem. Commun.* **2002**, 1240.
(27) Hoffmannova, H.; Fermín, D.; Krtil, P. *J. Electroanal. Chem.* **2004**, *562*, 261.
(28) Grabar, K. C.; Smith, P. C.; Musick, M. D.; Davis, J. A.; Walter, D. G.; Jackson, M. A.; Guthrie, A. P.; Natan, M. J. *J. Am. Chem. Soc.* **1996**, *118*, 1148.
(29) Takehara, K.; Takemura, H.; Ide, Y. *Electrochim. Acta* **1994**, *39*, 817.
(30) Benitez, G.; Vericat, C.; Tanco, S.; Lenicov, F. R.; Castez, M. F.; Vela, A. E.; Salvarezza, R. C. *Langmuir* **2004**, *20*, 5030.
(31) Arce, F. T.; Vela, M. E.; Salvarezza, R. C.; Arvia, A. J. *Langmuir* **1998**, *14*, 7203.
(32) Li, L.; Chen, S.; Jiang, S. *Langmuir* **2003**, *19*, 2974.
(33) Gorman, C. B.; He, Y.; Carroll, R. L. *Langmuir* **2001**, *17*, 5324.
(34) Azzaroni, O.; Vela, M. E.; Martin, H.; Creus, A. H.; Andreasen, G.; Salvarezza, R. C. *Langmuir* **2001**, *17*, 6647.
(35) Pardo-Yissar, V.; Katz, E.; Lioubashevski, O.; Willner, I. *Langmuir* **2001**, *17*, 1110.
(36) Huclova, S. Master Thesis, University of Berne, Berne, Switzerland, 2005.
(37) Amatore, C.; Saveant, J. M.; Tessier, D. *J. Electroanal. Chem.* **1983**, *147*, 39.
(38) Tokuda, K.; Gueshi, T.; Matsuda, H. *J. Electroanal. Chem.* **1979**, *102*, 41.
(39) Scharifker, B. R. *J. Electroanal. Chem*. **1988**, *240*, 61.
(40) Reincke, F.; Hickey, S. G.; Kelly, J. J.; Braam, T. W.; Jenneskens, L. W.; Vanmaekelbergh, D. *J. Electroanal. Chem.* **2002**, *522*, 2.
(41) Krysinski, P.; Brzostowska-Smolska, M. *J. Electroanal. Chem.* **1997**, *424*, 61.
(42) Janek, R. P.; Fawcett, W. R.; Ulman, A. *Langmuir* **1998**, *14*, 3011.
(43) Geblewicz, G.; Schiffrin, D. J. *J. Electroanal. Chem.* **1988**, *244*, 27.
(44) Peter, L. M.; Duerr, W.; Bindra, P.; Gerischer, H. *J. Electroanal. Chem*. **1976**, *71*, 31.
(45) Smalley, J. F.; Feldberg, S. W.; Chidsey, C. E. D.; Linford, M. R.; Newton, M. D.; Liu, Y.-P. *J. Phys. Chem.* **1995**, *99*, 13141.
(46) Slowinski, K.; Fong, H. K. Y.; Majda, M. *J. Am. Chem. Soc.* **1999**, *121*, 7257.
(47) Holmlin, R. E.; Ismagilov, R. F.; Haag, R.; Mujica, V.; Ratner, M. A.; Rampi, M. A.; Whitesides, G. M. *Angew. Chem., Int. Ed.* **2001**, *40*, 2316.
(48) Engelkes, V. B.; Beebe, J. M.; Frisbie, C. D. *J. Am. Chem. Soc.* **2004**, *126*, 14287.
(49) Frey, B. L.; Jordan, C. E.; Kornguth, S.; Corn, R. M. *Anal. Chem.* **1995**, *67*, 4452.
(50) Sur, U. K.; Lakshminarayanan, V. *J. Electroanal. Chem*. **2004**, *565*, 343.
(51) Barreira, S. V. P.; Garcia-Morales, V.; Pereira, C. M.; Manzanares, J. A.; Silva, F. *J. Phys. Chem. B* **2004**, *108*, 17973.
(52) Lee, S. Y.; Noh, J.; Ito, E.; Lee, H.; Hara, M. *Jpn. J. Appl. Phys.* **2003**, *42*, 236.
(53) Lee, S. Y.; Noh, J.; Hara, M.; Lee, H. *Mol. Cryst. Liq. Cryst.* **2002**, *377*, 177.
(54) Simmons, J. G. *J. Appl. Phys.* **1963**, *34*, 1793.